

Minimal d -Band Model for the Optical Susceptibility of Non-Centrosymmetric Monolayer Transition Metal Dichalcogenides

Angiolo Huamán¹

¹Department of Physics, University of Arkansas, Fayetteville, Arkansas 72701, USA

(Dated: December 30, 2025)

The optical response of two-dimensional (2D) materials has been customarily calculated *ab initio* using plane waves and without separating the most important orbitals contributions. In the family of transition metal dichalcogenides (TMDC) monolayers lacking inversion symmetry, we take advantage of the mostly d orbital content of the Bloch bands around the semiconductor gap to reduce the calculation of the linear and quadratic optical susceptibilities to a very minimal model. Such a simple approach reproduces well first principles calculations and could be the starting point for the inclusion of many-body effects and spin-orbit coupling (SOC) in TMDCs with only a few energy bands in a numerically inexpensive way.

I. INTRODUCTION

The optical response of solids, that is, the radiation fields emitted by them upon illumination, has been historically used to determine their structural and electronic properties, particularly their energy gaps [1]. Even though nowadays we have more precise techniques like ARPES, the study of the optical response, both at the experimental and theoretical level, is still of a fundamental importance.

Many different effects comprise the field of light-matter interaction, namely absorption by, transmission through, and reflection from the sample. In experiments dealing with the latter, the reflected patterns carry information about the structural properties of the material. This is more evident when the *nonlinear* response is detected: this is nonzero only when the underlying crystal lacks an inversion center, while the linear response is present regardless of the crystal geometry.

Calculations of the linear and nonlinear optical conductivity in non centrosymmetric materials have been mostly approached to by using first principle methods, such as density functional theory (DFT). However, DFT calculations have shown that the optical bands (those close to the energy gap) in 1T TMDCs are of a mostly d type, which poses the question of whether a calculation using this minimal basis is feasible and how it compares to more comprehensive approaches.

In this work, we build upon the three-band model with d orbitals by Liu *et al* [2] and calculate the linear and nonlinear (quadratic) optical susceptibility of non-centrosymmetric monolayer TMDC in the 2H stacking configuration, taking tungsten disulfide (WS₂) as an example, although the same calculation can be carried out for the entire family of TMDCs in [2]. Reflecting an almost complete d character of the energy bands around the energy gap, we see that the optical susceptibility thus obtained matches *ab initio* calculations for photon energies up to 1.7 eV above the band gap size. Using this simplified model as a basis, many-body effects can be added by using techniques based on tight-binding band structures [3].

This paper is organized as follows. Section II gives a brief description of monolayer TMDC in the 1T stacking. In Sec. (III) the basics of the formalism of the optical susceptibility in the single-particle approximation

are presented. Section IV is an account of the symmetry considerations leading to the reduction to the IBZ. In Sec. VI we present the formalism for the calculation of two-center integrals of the momentum operator. Section VII contains our results. The conclusions we arrived at are presented in Sec. VIII.

II. TMDC MONOLAYERS IN THE THREE-BAND APPROXIMATION

Monolayers of TMDCs can have an allotropic form with a D_{3h} point group, thus lacking an inversion center, as schematically shown in Figs. 1(a) and (b). The lattice vectors are chosen as $\mathbf{a}_1 = a\hat{x}$ and $\mathbf{a}_2 = a(\hat{x} + \sqrt{3}\hat{y})/2$, a being the lattice parameter. The transition metal atoms occupy the lattice sites while there are two chalcogens per primitive cell at positions $(1/3)(\mathbf{a}_1 + \mathbf{a}_2) \pm h\hat{z}/2$, where h is the chalcogen-chalcogen distance along the z direction. The reciprocal lattice vectors are $\mathbf{b}_1 = (4\pi/(a\sqrt{3}))(\sqrt{3}\hat{x} - \hat{y})/2$ and $\mathbf{b}_2 = (4\pi/(a\sqrt{3}))\hat{y}$, and the hexagonal Brillouin zone (BZ) is depicted in Fig. 1(c).

The mirror plane at the xy plane permits a decoupling between the two subsets of d -orbitals $\{d_{xy}, d_{z^2}, d_{x^2}\}$ and $\{d_{yz}, d_{xz}\}$, with different parity with respect to the operation $z \rightarrow -z$. Also, *ab initio* calculations have shown that the energy bands around the gap are mostly composed of orbitals of the former set, which allows the use of an effective three-band model as introduced by Liu *et al* [2], whose details are given in Appendix A.

Before going into the calculation of the optical susceptibility, in the next section we briefly review the main concepts and formulae.

III. OPTICAL SUSCEPTIBILITY IN THE SINGLE PARTICLE APPROXIMATION

We will work in the single-particle approximation and with an electromagnetic field with no spatial dependence, described by the vector potential $\mathbf{A}(t) = \mathbf{A}(\omega)e^{-i\omega t} + cc$. Although not explicitly written, ω is to be understood as a complex frequency $\omega + i\eta$, with η a small positive quantity

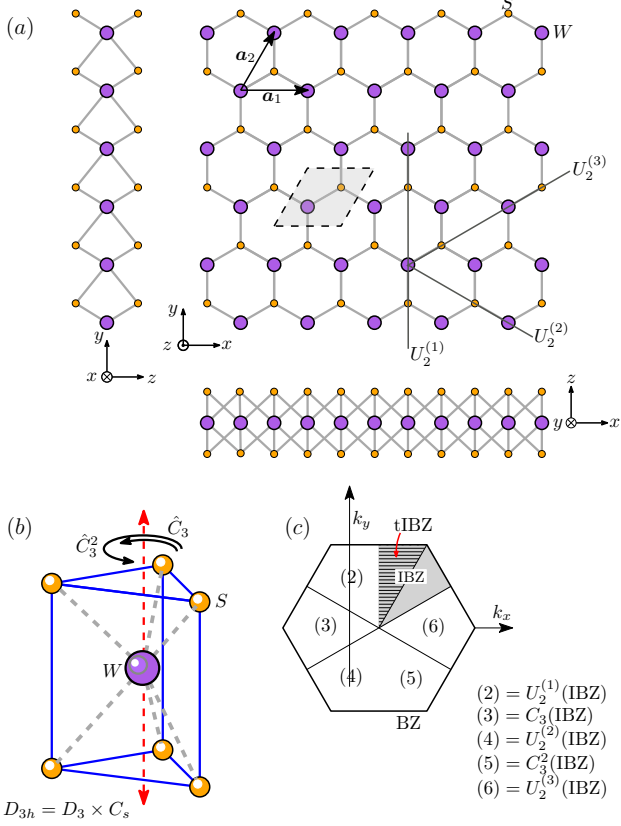


FIG. 1. (a) Top view of monolayer WS_2 with trigonal prismatic configuration $2H$ and lattice vectors \mathbf{a}_1 and \mathbf{a}_2 (lattice parameter $a = |\mathbf{a}_1| = |\mathbf{a}_2|$). Sulfur layers lie one on top of the other. (b) Trigonal unit cell of WS_2 exhibiting its D_{3h} symmetry. (c) Hexagonal first Brillouin zone (BZ), with the irreducible Brillouin zone (IBZ, gray shaded region) and time-reversed irreducible region (tIBZ, hatched area). Regions (2) through (6) are obtained from the IBZ by applying the symmetry operations indicated.

that guarantees that the vector potential $\mathbf{A}(t)$ vanishes at a remote past ($t \rightarrow -\infty$). The underlying monolayer TMDC under study is described by the static Hamiltonian $H_0 = \mathbf{p}^2/2m + V(\mathbf{r})$ [$V(\mathbf{r})$ is the self-consistent potential with the spatial symmetry of the crystal] with eigenvalues and Bloch eigenvectors satisfying $H_0\psi_{n\mathbf{k}} = \epsilon_n(\mathbf{k})\psi_{n\mathbf{k}}$, and that will be constructed using DFT with the SIESTA implementation. In the dipole approximation, the time-dependent Hamiltonian of the material coupled to the optical field, $H(t)$, can be obtained using the Peierls substitution and keeping only terms linear in the vector potential $\mathbf{A}(t)$:

$$H(t) = [\mathbf{p} + e\mathbf{A}(t)]^2/2m + V(\mathbf{r}) \simeq H_0 + H_1(t) + \mathcal{O}(A^2), \quad (1)$$

with $H_1(t) = (e/m)\mathbf{A}(t) \cdot \mathbf{p}$ ($-e$ is the electron charge). The theory of the linear and nonlinear optical susceptibilities is abundant [4–7], so in what follows we will summarize the main concepts and equations.

A. Linear optical susceptibility

For monochromatic illumination, the single-body linear optical susceptibility tensor $\chi_{ij}^{(1)}(\omega)$ in SI units is dimensionless and given in terms of the Fourier components of the induced polarization $\mathbf{P}(t)$ and the applied electric field $\mathbf{E}(t)$ [4, 8]:

$$P_i(\omega) = \epsilon_0 \chi_{ij}^{(1)}(\omega) E_j(\omega), \quad (2)$$

with $\mathbf{E}(\omega) = i\omega \mathbf{A}(\omega)$. The optical susceptibility is obtained by solving the density matrix in a perturbative way, and from it the macroscopic induced current $\mathbf{J}(t)$. The macroscopic polarization is obtained through $\mathbf{P}(t) = \int_{-\infty}^t d\tau \mathbf{P}(\tau)$ [9], up to the linear order in $\mathbf{A}(t)$, as shown elsewhere [4]. Considering only interband transitions we get the following expression:

$$\chi_{ij}^{(1)}(\omega) = \frac{e^2 \hbar^2}{\epsilon_0 m^2} \frac{1}{V} \sum_{\mathbf{k}} \sum_{v,c} \frac{p_{vc}^i p_{cv}^j}{\epsilon_{cv}^2 (\epsilon_{cv} - \hbar\omega - i\eta)}, \quad (3)$$

with $\epsilon_{cv} = \epsilon_c - \epsilon_v$, $p_{vc}^i = \langle \psi_v | p^i | \psi_c \rangle$, p^i is the i -th component of the momentum operator, m is the electron mass and V is the volume of the sample. The imaginary part in ω has been explicitly written. The \mathbf{k} -dependence on the energy bands and Bloch eigenstates is dropped not to load the notation. The sums run over valence (v) and conduction (c) Bloch eigenstates of H_0 . Following Ref. [10], in the monolayer limit the Bloch wavefunctions are highly localized at $z = 0$ (the plane of the monolayer), so the sum over k_z can be replaced with N_z , where N_z is the number of monolayers in the sample. If the interlayer distance is a_3 , the volume V can be written as $V = N_z a_3 S$, where S is the area of the layer. After passing to the continuous limit in the in-plane coordinates k_x and k_y , we get:

$$\chi_{ij}^{(1)}(\omega) = \frac{1}{a_3} \frac{e^2 \hbar^2}{\epsilon_0 m^2} \int_{\text{BZ}} \frac{d\mathbf{k}}{(2\pi)^2} \times \sum_{v,c} \frac{p_{vc}^i p_{cv}^j}{\epsilon_{cv}^2 (\epsilon_{cv} - \hbar\omega - i\eta)}, \quad (4)$$

where the integral is over the two-dimensional Brillouin zone (BZ). The expression in Eq. (4) can be recast by using time reversal symmetry, which implies that $(p_{vc}^i(\mathbf{k}))^* = -p_{vc}^i(-\mathbf{k})$, and allows to get its imaginary part by using the property $1/(x \pm i\eta) = \mathcal{P}(1/x) \mp i\pi\delta(x)$ (\mathcal{P} is the Cauchy principal part [11]):

$$\text{Im}[\chi_{ij}^{(1)}(\omega)] = -\frac{1}{a_3} \frac{\pi e^2 \hbar^4}{\epsilon_0 m^2} \times \sum_{v,c} \int_{\text{BZ}} \frac{d\mathbf{k}}{(2\pi)^2} \frac{\text{Re}[\zeta_{cv}^i \zeta_{cv}^j]}{\epsilon_{cv}^2} \delta(\epsilon_{cv} - \hbar\omega). \quad (5)$$

In the expression above we have defined the matrix elements of the derivatives $\partial/\partial x_a$:

$$\zeta_{cv}^a(\mathbf{k}) = \int d\mathbf{r} \psi_{ck}^* \frac{\partial}{\partial x_a} \psi_{vk}. \quad (6)$$

The Dirac delta in Eq. (5) allows to pull the factor $1/\epsilon_{cv}^2$ out of the integral and make it equal to $1/\omega^2$. We have verified the difference between both calculations lies within the numerical error. For this equation it might also be useful to keep in mind that $e^2\hbar^4/\epsilon_0 m^2 \simeq 1.1 \times 10^4 \text{ eV}^3 \text{ \AA}^5$. The complex dielectric function is defined as $\epsilon_{ij}(\omega) = \epsilon'_{ij} + i\epsilon''_{ij} = \delta_{ij} + \chi_{ij}^{(1)}$, δ_{ij} being the Kronecker symbol. Once having $\chi_{ij}^{(1)}$, related linear quantities such as refractive index, reflectivity, and absorption spectrum can be calculated. The integration of Eq. (5) has been accomplished by a *broadening* method consisting in replacing $\delta(\epsilon_{cv} - \hbar\omega)$ with a Gaussian function of a small width [12]. This approach results in a smoother dispersion of the susceptibility at the expense of a denser integration mesh, compared to other approaches such as the linear tetrahedral method [13]. In Sec. VII we give more details on the our integration procedure.

B. Second order susceptibility

The second order susceptibility tensor $\chi_{ijk}^{(2)}$ is defined in S.I. units as follows [14, 15]:

$$P_i(\omega) = \epsilon_0 \chi_{ijk}^{(2)}(\omega) E_j(\omega) E_k(\omega). \quad (7)$$

From this definition it follows that $\chi_{ijk}^{(2)}$ is symmetric in its last two indices, $\chi_{ijk}^{(2)} = \chi_{ikj}^{(2)}$, and that has dimensions of length over voltage. The expression for $\chi_{ijk}^{(2)}$ in terms of eigenstates and energy bands of H_0 is obtained in a similar manner as for $\chi_{ij}^{(1)}$, this time by expanding the density matrix up to second order in the vector potential $\mathbf{A}(t)$. This procedure is rather lengthy but has been explored abundantly in the literature [4–7], so here we will present the final formulae only.

It is convenient to write $\chi_{ijk}^{(2)}$ as a sum of two terms, $\chi_{ijk}^{(2)} = A_{ijk} + B_{ijk}$, each one symmetric in its last two indices and with imaginary parts given by [4]:

$$\text{Im}[A_{ijk}] = \frac{1}{a_3} \frac{e^3 \hbar^6}{2\epsilon_0 m^3} \int \frac{d\mathbf{k}}{(2\pi)^2} \sum_{v,c} \frac{16\pi}{\epsilon_{cv}^3} \delta(\epsilon_{cv} - 2\hbar\omega) \left(\sum_{v'} \frac{\text{Im}[i\zeta_{vc}^i \{\zeta_{cv'}^j, \zeta_{v'v}^k\}]}{2\epsilon_{cv'} - \epsilon_{cv}} - \sum_{c'} \frac{\text{Im}[i\zeta_{vc}^i \{\zeta_{cc'}^j, \zeta_{c'v}^k\}]}{2\epsilon_{c'v} - \epsilon_{cv}} \right), \quad (8)$$

$$\text{Im}[B_{ijk}] = \frac{1}{a_3} \frac{e^3 \hbar^6}{2\epsilon_0 m^3} \int \frac{d\mathbf{k}}{(2\pi)^2} \sum_{v,c} \frac{\pi}{\epsilon_{cv}^3} \delta(\epsilon_{cv} - \hbar\omega) \left(\sum_{n \neq c} \frac{\text{Im}[i\zeta_{nc}^i \{\zeta_{cv}^j, \zeta_{vn}^k\}]}{\epsilon_{cn} - 2\epsilon_{cv}} - \sum_{n \neq v} \frac{\text{Im}[i\zeta_{vn}^i \{\zeta_{nc}^j, \zeta_{cv}^k\}]}{\epsilon_{nv} - 2\epsilon_{cv}} \right). \quad (9)$$

In these expressions we have introduced the *symmetrizing* operator $\{R^j, L^k\} = (R^j L^k + R^k L^j)/2$, that enforces the symmetry $\chi_{ijk}^{(2)} = \chi_{ikj}^{(2)}$. It might be useful to remember that $e^3 \hbar^6/\epsilon_0 m^3 \simeq 8.1 \times 10^4 \text{ \AA}^7 \text{ eV}^5/\text{V}$. As with the linear susceptibility, $\chi_{ijk}^{(2)}$ has been scaled with the interlayer distance by the factor $1/a_3$. Also, the separation into Eqs. (8) and (9) is more than just formal: the different Dirac deltas in Eq. (8) and (9) are treated differently when doing the integration over the Brillouin zone. Similarly to the linear susceptibility, the denominators ϵ_{cv}^3 are constant over the surface of integration determined by the Dirac deltas and can be pulled out of the integral.

Both Eq. (5) and Eqs. (8) and (9) depend on momentum matrix elements and an integration over the whole BZ in their definitions. In the next section we present an explicit development of the symmetry arguments leading to the integration over a reduced part of the Brillouin zone.

IV. SYMMETRY OF THE BLOCH EIGENSTATES AS COMBINATIONS OF PSEUDO ORBITALS

The symmetry properties of the Bloch eigenstates and energy bands is fundamental to reduce the integration region in \mathbf{k} –space and to guarantee the convergence of the nonzero entries in both $\chi_{ij}^{(1)}$ and $\chi_{ijk}^{(2)}$. These include both to the spatial symmetries corresponding to the material’s crystal class and time reversal (which is a property of H_0 , and not of $H(t)$ in general).

Equations (5), (8) and (9) contain matrix elements of the momentum operator between Bloch eigenstates, the latter of which have not been constructed yet. In this sections we address that point. These Bloch eigenstates for the non illuminated WS₂ can be expanded, as an approximation, in a basis of pseudo atomic orbitals obtained from DFT. Liu *et al* [16] have shown that the broad family of TMDC MX₂ monolayers (M=W, Mo and X=S, Se, Te) in the trigonal prismatic configuration [i.e., without an inversion center, see Fig. 1(b)] can be described by using only *d*–orbitals of the transition metal if the bands around the semiconductor gap

(which are the most relevant for optical excitations) are to be correctly described. Moreover, because of the σ_h symmetry present in their D_{3h} point group, only d -orbitals even in z , that is, d_{xy} , d_{x^2} or d_{z^2} , have to be included. Calculation using DFT with plane waves show that the orbital content of the three bands closest to the energy gap are precisely of this d kind. For each pseudo atomic orbital d_{xy} , d_{x^2} or d_{z^2} in the primitive cell, the periodic part of the Bloch orbital can be written as follows:

$$u_{n\mathbf{k}}(\mathbf{r}) = \frac{1}{\sqrt{N}} \sum_{\mathbf{R}} e^{i\mathbf{k}\cdot(\mathbf{R}-\mathbf{r})} \varphi_n(\mathbf{r}-\mathbf{R}), \quad (10)$$

where the sum is over the N lattice sites $\mathbf{R} = \sum_j n_j \mathbf{a}_j$ (n_j integers) comprising the sample. The full Bloch orbital is $\varphi_{n\mathbf{k}}(\mathbf{r}) = e^{i\mathbf{k}\cdot\mathbf{r}} u_{n\mathbf{k}}(\mathbf{r})$. As customary, the matrix elements of the TB Hamiltonian matrix are taken between these Bloch orbitals $\varphi_{n\mathbf{k}}(\mathbf{r})$:

$$H_{0,ab}(\mathbf{k}) = \int d\mathbf{r} \varphi_{ak}^*(\mathbf{r}) H_0(\mathbf{r}) \varphi_{bk}(\mathbf{r}). \quad (11)$$

If we restrict \mathbf{k} in Eq. (11) to be in the IBZ, $H_{0,ab}(\mathbf{k})$ for other \mathbf{k} points can be directly obtained. To this, let \hat{G} be a symmetry operation belonging to the group D_{3h} . Performing the substitution $\mathbf{r} \rightarrow \hat{G}\mathbf{r}$ in the integral in Eq. (11) it can be shown that:

$$H_{0,ab}(\hat{G}\mathbf{k}) = G_{\mu a} H_{0,\mu\nu}(\mathbf{k}) G_{\nu b}, \quad (12)$$

where $G_{\mu\nu}$ are the entries of the orthogonal matrix of \hat{G} in the representation given by orbitals $\{d_{z^2}, d_{xy}, d_{x^2}\} = \{d_1, d_2, d_3\}$, that is, $d_\alpha(\hat{G}\mathbf{r}) = G_{\beta\alpha} d_\beta(\mathbf{r})$. This representation is reducible and can be written as $A'_1 + E'$ [17]. The form of the G matrices can be worked out by noticing that $D_{3h} = D_{3d} \times C_s$ [18], where C_s is the point group containing only the identity and the reflection σ_h in the xy plane (the plane of the monolayer). This operation has the only effect of changing z with $-z$, and becomes redundant in our two-dimensional representation of \mathbf{k} -space. Since the full 2D FBZ can be fully covered using the D_{3d} operation, only the representations of the latter will be necessary. It is clear that all of these operations satisfy $d_{z^2}(\hat{G}\mathbf{r}) = d_{z^2}(\mathbf{r})$. Thus, if the symmetry operations \hat{G} of D_{3d} in Cartesian space are written as:

$$\begin{pmatrix} g_{11} & g_{12} & 0 \\ g_{21} & g_{22} & 0 \\ 0 & 0 & \pm 1 \end{pmatrix} \quad (13)$$

their correspondent G matrices in the basis $\{d_{z^2}, d_{xy}, d_{x^2}\} = \{d_1, d_2, d_3\}$ are:

$$G = \begin{pmatrix} 1 & 0 & 0 \\ 0 & g_{11}g_{22} + g_{12}g_{21} & 2g_{11}g_{12} \\ 0 & 2g_{11}g_{21} & g_{11}^2 - g_{21}^2 \end{pmatrix}. \quad (14)$$

With the expression above, Eq. (12) can be written in matrix form as $H_0(\hat{G}\mathbf{k}) = G^T H_0(\mathbf{k}) G$. Since every point in

the FBZ can be obtained from another one in the IBZ upon application of a suitably chosen \hat{G} operation, the TB Hamiltonian matrix given in Eq. (11) for points in the IBZ have to be numerically diagonalized.

Let us pass to the calculation of the matrix elements of the momentum operator. Customarily, these have been based on the projector-augmented wave (PAW) method [19]. In our case, the Bloch eigenstates of H_0 (see Sec. III) in the \mathbf{r} -representation can be expanded as a combination of Bloch orbitals:

$$\psi_{n\mathbf{k}}(\mathbf{r}) = \sum_s C_{sn}(\mathbf{k}) \varphi_{s\mathbf{k}}(\mathbf{r}), \quad (15)$$

the matrix elements $C_{sn}(\mathbf{k})$ are obtained by diagonalizing the tight-binding Hamiltonian Eq. (11) with DFT parameters, resulting in $H_0(\mathbf{k}) C(\mathbf{k}) = C(\mathbf{k}) \epsilon(\mathbf{k})$, where $\epsilon(\mathbf{k})$ is a diagonal matrix with $\epsilon_{ab}(\mathbf{k}) = \epsilon_a(\mathbf{k}) \delta_{a,b}$, containing the energy bands. This relation, together with Eq. (11), allow us to choose the gauge $C(\hat{G}\mathbf{k}) = G^T C(\mathbf{k})$, for \mathbf{k} in the IBZ. Moreover, with this choice it is guaranteed the well known property in Bloch theory [20]:

$$\psi_{n\mathbf{k}}(\hat{G}\mathbf{r}) = \psi_{n\hat{G}^{-1}\mathbf{k}}(\mathbf{r}), \quad (16)$$

for non-degenerate energy bands. The matrix elements $p_{ab}^i(\mathbf{k})$ of the momentum operator are more conveniently written as $p_{ab}^i(\mathbf{k}) = (\hbar/2i) \zeta_{ab}^i(\mathbf{k})$, where $\zeta_{ab}^i(\mathbf{k})$ are matrix elements of the derivative operator $\partial/\partial x^i$ and can be written using Eqs. (10) and (15) as follows:

$$\zeta_{ab}^{(j)}(\mathbf{k}) = \sum_{s,s'} C_{sa}^*(\mathbf{k}) C_{s'b}(\mathbf{k}) \sum_{\mathbf{R}} e^{-i\mathbf{k}\cdot\mathbf{R}} D_{ss'}^{(j)}(\mathbf{R}). \quad (17)$$

The quantity $D_{ss'}^{(j)}(\mathbf{R})$ is a two-center integral of the derivative operator between localized pseudo orbitals separated by \mathbf{R} :

$$D_{ss'}^{(j)}(\mathbf{R}) = \int d\mathbf{r} \varphi_s(\mathbf{r}-\mathbf{R}) \frac{\partial}{\partial x^j} \varphi_{s'}(\mathbf{r}). \quad (18)$$

Integrating by parts the equation above and keeping in mind the parity of the d -orbitals, it is easy to verify its symmetry, i.e.,

$$D_{ss'}^{(j)}(\mathbf{R}) = D_{s's}^{(j)}(\mathbf{R}). \quad (19)$$

It might be useful to notice that, defining matrices $\zeta^{(j)}(\mathbf{k})$ and $D^{(j)}(\mathbf{R})$ with entries $\zeta_{ab}^{(j)}(\mathbf{k})$ and $D_{ss'}^{(j)}(\mathbf{R})$ respectively, Eq. (17) can be recast as $\zeta^{(j)}(\mathbf{k}) = \sum_{\mathbf{R}} e^{-i\mathbf{k}\cdot\mathbf{R}} C^\dagger(\mathbf{k}) D^{(j)}(\mathbf{R}) C(\mathbf{k})$.

Before moving forward, it is informative to state the transformation rules of Eq. (17) under D_{3h} symmetries. Replacing \mathbf{k} with $\hat{G}\mathbf{k}$ (\hat{G} belonging to D_{3h}) and using the facts that $C(\hat{G}\mathbf{k}) = G^T C(\mathbf{k})$ and $d_\alpha(\hat{G}\mathbf{r}) = G_{\beta\alpha} d_\beta(\mathbf{r})$, it can be shown that:

$$\zeta_{\mu\nu}^{(j)}(\hat{G}\mathbf{k}) = M_{ji} \zeta_{\mu\nu}^{(i)}(\mathbf{k}) \quad (20)$$

where M_{ji} is the matrix representation of \hat{G} in the basis Cartesian basis $\{x, y, z\}$ (M_{ji} should not be confused with G_{ji}).

V. NONZERO COMPONENTS OF $\chi_{ij}^{(1)}$ AND $\chi_{ijk}^{(2)}$

As it is well known, the point group of a crystal (its crystal class), greatly constrains the nonzero elements of its optical susceptibility at any order [14, 21]. For the linear susceptibility, this is most easily seen by means of the substitution $\mathbf{k} \rightarrow \hat{G}\mathbf{k}$ in Eq. (4), which does not affect either the size or the shape of the BZ since the latter has all the symmetries of the D_{3h} point group. Using the transformation in Eq. (20) we get:

$$\chi_{ij}^{(1)} = M_{im} M_{jn} \chi_{mn}^{(1)}, \quad (21)$$

which constitutes a homogeneous system of $n_{D_{3h}}$ linear algebraic equations, $n_{D_{3h}} = 12$ being the order of the D_{3h} point group, each equation corresponding to one symmetry operation. Upon consecutive application of all the symmetry operations in D_{3h} it can be verified the following [x , y and z subscripts indicate Cartesian coordinates according to Fig. 1(a)]:

$$\chi_{xx}^{(1)} = \chi_{yy}^{(1)}, \quad (22)$$

all other entries being zero. The same symmetries, along with time reversal, help us reduce the integral over the BZ to only its time-reversed irreducible part [tIBZ, see Fig. 1(c)]. To this end, we follow a symmetrizing strategy [22]. For the linear susceptibility, the integral in Eq. (4) can be written in the following fashion:

$$\text{Im}[\chi_{ij}^{(1)}(\omega)] = -\frac{1}{a_3} \frac{\pi e^2 \hbar^4}{\varepsilon_0 m^2} \sum_{v,c} \int_{\text{BZ}} \frac{d\mathbf{k}}{(2\pi)^2} \times \sum_{\hat{G}} \text{Re}[\zeta_{vc}^i(\hat{G}\mathbf{k}) \zeta_{cv}^j(\hat{G}\mathbf{k})] / g \frac{\delta(\epsilon_{cv} - \hbar\omega)}{\epsilon_{cv}^2}, \quad (23)$$

where the sum over \hat{G} extends to all the symmetry operations in the point group D_3 (the C_s part in the decomposition $D_{3h} = D_3 \times C_s$ becomes redundant in our 2D approximation) and $g = 6$ is the order of D_3 . In this way, the integrand in Eq. (23) has the full D_3 symmetry, and thus can be reduced to an integral over the IBZ times g . Time-reversal symmetry allows for a further reduction to the tIBZ times two. Thus, Eq. (23) goes over into:

$$\text{Im}[\chi_{ij}^{(1)}(\omega)] = -\frac{2}{a_3} \frac{\pi e^2 \hbar^4}{\varepsilon_0 m^2} \times \sum_{v,c} \int_{\text{tIBZ}} \frac{d\mathbf{k}}{(2\pi)^2} \frac{\sum_{\hat{G}} \text{Re}[\zeta_{vc}^i(\hat{G}\mathbf{k}) \zeta_{cv}^j(\hat{G}\mathbf{k})]}{\epsilon_{cv}^2} \delta(\epsilon_{cv} - \hbar\omega), \quad (24)$$

By using Eq. (20), the integral in the equation above can be written as combinations of integrals of the kind in Eq. (5) but over the tIBZ. More precisely, this can be done by using the transformation law:

$$\zeta_{vc}^i(\hat{G}\mathbf{k}) \zeta_{cv}^j(\hat{G}\mathbf{k}) = M_{il} M_{jp} \zeta_{vc}^l(\mathbf{k}) \zeta_{cv}^p(\mathbf{k}) \quad (25)$$

By means of this $\chi_{xx}^{(1)}$ can be written as a combination of integrals over the tIBZ only :

$$\text{Im}[\chi_{xx}^{(1)}(\omega)] = -6 \frac{\pi e^2 \hbar^4}{\varepsilon_0 m^2} \left[\int_{\text{tIBZ}} \frac{d\mathbf{k}}{(2\pi)^2} \sum_{v,c} \frac{\zeta_{vc}^x \zeta_{cv}^x}{\epsilon_{cv}^2} \delta(\epsilon_{cv} - \hbar\omega) + \int_{\text{tIBZ}} \frac{d\mathbf{k}}{(2\pi)^2} \sum_{v,c} \frac{\zeta_{vc}^y \zeta_{cv}^y}{\epsilon_{cv}^2} \delta(\epsilon_{cv} - \hbar\omega) \right], \quad (26)$$

Exactly the same equation holds true for $\chi_{yy}^{(1)}$, as it should. All other components are zero and $\chi_{zz}^{(1)}$ is also so because of the mirror plane normal passing through the transition metal atoms.

While bulk TMDCs do not have a second-order nonlinear susceptibility because of its D_{6h} point group, which contains inversion as one of its symmetries, TMDCs monolayer have a reduced D_{3h} point group with no inversion operation. For the second order susceptibility a similar result holds, namely:

$$\chi_{ijk}^{(2)} = M_{im} M_{jn} M_{kl} \chi_{mnl}^{(2)}. \quad (27)$$

Because of σ_h mirror in the xy plane along with the σ_1 all the components with at least a z index are zero. Applying all the other symmetries we get:

$$\chi_{xxy}^{(2)} = \chi_{yxx}^{(2)} = -\chi_{yyy}^{(2)}. \quad (28)$$

Similarly to the linear case, the integrand in Eqs. (8) and (9) can be symmetrized, thus reducing the integral over the whole BZ to the tIBZ. Without going into details, the final result is:

$$\chi_{xxy}^{(2)} = 2 \left[3\bar{\chi}_{xxy}^{(2)} + \frac{3}{2} (\bar{\chi}_{yxx}^{(2)} - \bar{\chi}_{yyy}^{(2)}) \right], \quad (29)$$

where the bars over the expressions in the rhs of the equation above mean that they are to be calculated using Eqs. (8) and (9) but with an integration over the tIBZ only. It must be emphasised that Eq. (26) and (29) are in no way particular to TMDCs, but follow directly from the D_{3h} symmetry and thus apply equally to any 2D material belonging to this crystal class.

The numerical evaluation of two-center integrals of the like of Eq. (18) is a recurrent problem in DFT and related areas. Inspired in the Slater-Koster approach [23], we combine the intrinsic symmetries of d -orbitals upon orthogonal transformations with an axes rotation to bring Eq. (18) to a combination of just a few numerically evaluated integrals, as explained next.

VI. TWO-CENTER INTEGRALS OF THE MOMENTUM OPERATOR

Here, instead of calculating all the integrals in Eq. (18) numerically, we perform an axes rotation that brings \mathbf{R} into the \hat{x} direction. In this configuration, the integrals $d_{ss'}(a_p \hat{x})$ (a_p is the magnitude of \mathbf{R} , that will depend on whether we

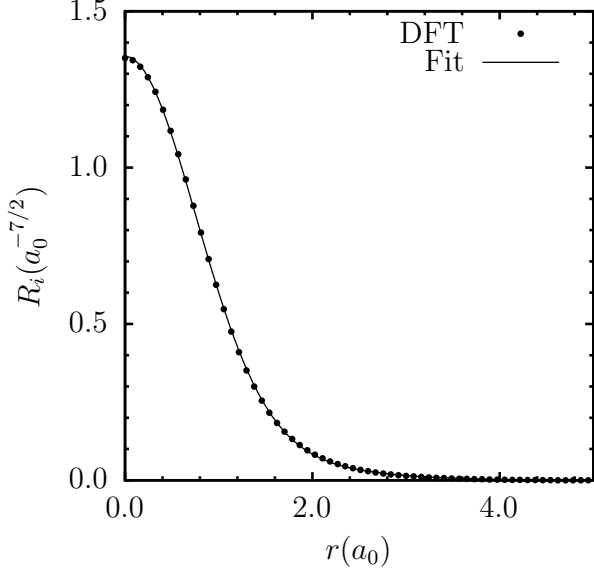


FIG. 2. Radial part of the d pseudo orbitals for tungsten. The dots are the DFT data while the solid line is the fitting in Eq. (33) (a_0 is the Bohr radius).

are dealing with nearest, second nearest and third nearest atomic neighbors) are not all independent, but only a few of them have to be numerically evaluated. The final values of Eq. (18) are obtained by bringing back the x axis to $\mathbf{R} - \delta_{s'} + \delta_s$ and using the fact that atomic pseudo orbitals corresponding to the same angular momentum l transform into each other. This approach reduces the computational effort by minimizing the number of numerical integration. For the few integrals that have to be numerically calculated, we used the Gauss-Legendre quadrature over a box centered at the midpoint of \mathbf{R} and with dimensions $(a_p + 2R_c) \times R_c \times R_c$, where R_c is slightly larger than the maximum radial extension of the pseudo orbitals (in our case, roughly 4 Å, corresponding to the d -orbitals of tungsten; see Fig. 2).

This general two-center integral can be reduced to combinations of simpler integrals by rotating the coordinate system such that the new axis x is made to coincide with the direction \mathbf{R} . In the monolayer limit, these rotations are only in-plane, so the general vector \mathbf{R} can be written as $\mathbf{R} = a_p(\cos \phi \hat{\mathbf{x}} + \sin \phi \hat{\mathbf{y}})$, the matrix performing this rotation is:

$$M(\mathbf{R}) = \begin{pmatrix} \cos \phi & -\sin \phi & 0 \\ \sin \phi & \cos \phi & 0 \\ 0 & 0 & 1 \end{pmatrix}. \quad (30)$$

For a given value of a_p , only the matrix elements $D_{11}^{(1)}(a_p \hat{\mathbf{x}})$, $D_{22}^{(1)}(a_p \hat{\mathbf{x}})$, $D_{33}^{(1)}(a_p \hat{\mathbf{x}})$, $D_{13}^{(1)}(a_p \hat{\mathbf{x}})$, $D_{12}^{(2)}(a_p \hat{\mathbf{x}})$ and $D_{23}^{(2)}(a_p \hat{\mathbf{x}})$ are needed, supplemented with the identity Eq. (19). Because of the σ_h symmetry, all $D_{ss'}^{(3)}(a_p \hat{\mathbf{x}})$ are zero, which in turn will result in $\chi_{ij}^{(1)} = 0$ and $\chi_{ijk}^{(2)} = 0$ if at least one of its indices is z . The general integral in Eq. (18) can

thus be written as:

$$D_{ss'}^{(j)}(\mathbf{R}) = M_{d,as} M_{ji} M_{d,bs'} \times \int d\mathbf{r} \varphi_a(\mathbf{r} - a_p \hat{\mathbf{x}}) \frac{\partial}{\partial x^i} \varphi_b(\mathbf{r}), \quad (31)$$

where M_d is the transformation matrix of the rotation in Eq. (30) of the d -orbitals:

$$M_d(\mathbf{R}) = \begin{pmatrix} 1 & 0 & 0 \\ 0 & \cos 2\phi & \sin 2\phi \\ 0 & -\sin 2\phi & \cos 2\phi \end{pmatrix}. \quad (32)$$

The radial part of the d -orbitals are obtained from DFT calculations using the SIESTA package [24], and it is written as $R(r) = r^2 R_i(r)$, where R_i is given by the SIESTA output. It is given as a table but we verified that it can be fitted to Gaussian functions. In our case, two Gaussians were sufficient:

$$R_i(r) = a_1 e^{-b_1 r^2} + a_2 e^{-b_2 r^2}, \quad (33)$$

with parameters $a_1 = 0.135064 a_0^{-7/2}$, $b_1 = 0.244444 a_0^{-1}$, $a_2 = 1.22115 a_0^{-7/2}$ and $b_2 = 0.904556 a_0^{-1}$, fitted from DFT pseudo orbitals (a_0 is the Bohr radius). The fitted equation is normalized to 0.001%, so we renormalize it again. The form of the Eq. (33) has the advantage that $(1/r) dR_i/dr$ is well behaved at the origin, which simplifies the numerical implementation of the derivatives in Eq. (18). Figure 2 shows the DFT data (dots) and the fitting in Eq. (33) (solid line).

For the six integrals that have to be numerically evaluated, the Gauss-Legendre quadrature with a fine grid over a rectangular parallelepiped centered at the midpoint of $\mathbf{R} = a_p \hat{\mathbf{x}}$ with ranges $-a_m \leq x \leq a_p + a_m$, $-a_m \leq y \leq a_m$ and $-a_m \leq z \leq a_m$ was used, where a_m is a positive quantity larger than r_c , the maximum spatial extension of the radial parts among the PAOs, to guarantee an appropriate convergence.

VII. RESULTS

Liu *et al* [2] have fitted the TB parameters of the whole family of 2H TMDCs monolayer at the high symmetry K point to correctly describe the energy gap, so there is no need to introduce corrections by the overlap matrix or a scissors operator [4]. A summary of the model including third nearest neighbors is given in Appendix A. The energy bands are shown in Fig. 3 along with the ones with nearest neighbors, for the sake of comparison. As it can be seen, both NN and TNN approximations coincide in a very small vicinity of the K point, although they sharply diverge away from it. As shown in [2], the TNN approximation describes well the topmost valence and two bottommost conduction bands throughout the BZ. Since optical excitations occur mostly in this energy region, a model of the optical susceptibility in this energy range is justified.

The imaginary part of the optical susceptibility, Eqs. (26) and (29), was integrated by means of a Gaussian broadening

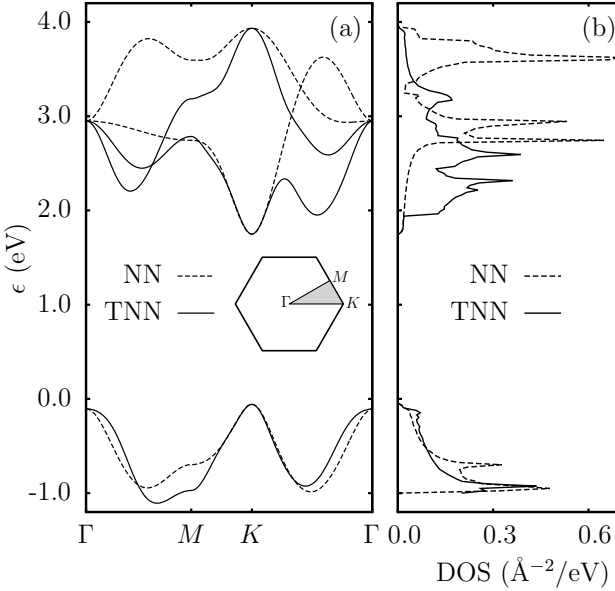


FIG. 3. (a) Energy bands of monolayer WS₂ in the nearest (NN, dashed line) and third nearest (TNN, solid line) neighbors approximation with TB parameters from [2], along the path $\Gamma \rightarrow M \rightarrow K \rightarrow \Gamma$ in the BZ. (b) Density of states corresponding to the bands in (a), calculated using the 2D linear tetrahedral method.

approach. The Dirac delta is written as $\delta(\epsilon_{cv} - s\hbar\omega) = \delta(w \times (\epsilon_{cv} - s\hbar\omega)/w) = (1/w)\delta((\epsilon_{cv} - s\hbar\omega)/w)$, where $s = 1, 2$ [see Eqs. (8) and (9)], and w is a positive energy making the argument in the Dirac delta dimensionless and giving the broadening of it. The latter is approximated using [25]:

$$\delta(x) = \sum_{n=0}^N A_n H_{2n}(x) e^{-x^2}, \quad (34)$$

with $A_n = (-1)^n / (n! 4^n \sqrt{\pi})$. We have verified that dividing the tIBZ into 1275 cells of equal size and shape, and setting $w = 0.1$ eV and $N = 3$, convergence in both $\chi_{ij}^{(1)}$ and $\chi_{ijk}^{(2)}$ is achieved. Also, because of the smallness of our system, full BZ integrations were also performed, with agreement between each other also with the relations in Eq. (22) and (29), within a small degree of numerical noise. The real part of both $\chi_{ij}^{(1)}$ and $\chi_{ijk}^{(2)}$ is calculated from the imaginary one by means of the Kramers-Kronig relations [26]:

$$\text{Re}[\chi_{ij}^{(1)}(\omega)] = \frac{1}{\pi} \mathcal{P} \int_{-\infty}^{+\infty} \frac{\text{Im}[\chi_{ij}^{(1)}(\omega')]}{\omega' - \omega} d\omega', \quad (35)$$

(\mathcal{P} indicates that the integral is to be evaluated as its principal part [11]).

Figure 4(a) shows the imaginary (solid line) and real (dashed line) parts of the only independent component of the linear optical susceptibility, $\chi_{xx}^{(1)}$. Because WS₂ monolayer has a direct band gap, the onset of $\text{Im}[\chi_{ij}^{(1)}]$ appears for energies greater than the gap size, $\min[\epsilon_{cv}(\mathbf{k})]$, indicated by the vertical dotted line in Fig. 4(a). The local maxima at energies roughly equal to 1.86 eV, 2.73 eV and 3.06

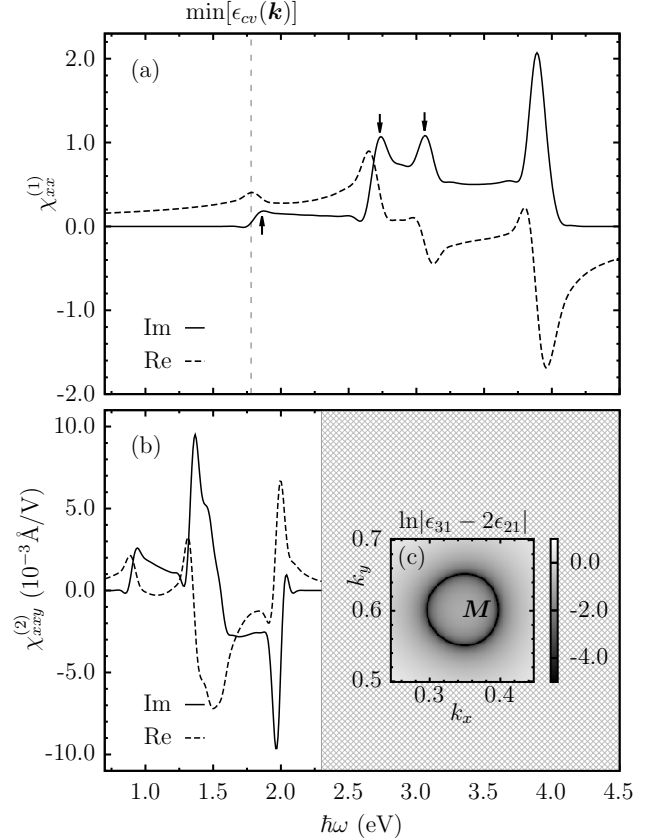


FIG. 4. (a) Imaginary and real parts of the $\chi_{xx}^{(1)}$ component of monolayer WS₂ as a function of the photon energy $\hbar\omega$. (b) Same as in (a) but for the $\chi_{xxy}^{(2)}$ of the nonlinear susceptibility. For $\chi_{xxy}^{(2)}$, photon energies up to 2.3 eV has been included only. (c) Logarithm of the energy difference $\ln|\epsilon_{31} - 2\epsilon_{21}|$ showing that it vanishes in a almost circular ring around M point.

eV (indicated by arrows) have been reported before using *ab initio* calculations with the projector augmented-wave method [27]. However, the sharp maximum around 4 eV has been shown to be smaller than the ones around 2.73 eV and 3.06 eV. This discrepancy might have its origin in the small number of bands we are using: since $\chi_{ij}^{(1)}$ depends on $\delta(\epsilon_{cv} - \hbar\omega)$, the higher the photon energy $\hbar\omega$, the more conduction bands are needed to match the condition $\epsilon_{cv} = \hbar\omega$. In this regard, we can say that the three band approximation gives reliable results up to, say, 3.5 eV.

Figure 4(b) shows the imaginary and real parts of $\chi_{xxy}^{(2)}$ [see Eq. (29)]. We present results only in the energy range $0.7 \text{ eV} \leq \hbar\omega \leq 2.3 \text{ eV}$. Because the $\delta(\epsilon_{cv} - 2\hbar\omega)$ in Eq. (8), the onset of second order susceptibility is now $\min[\epsilon_{cv}(\mathbf{k})]/2$. The contribution $\text{Im}[B_{ijk}]$ from Eq. (9), that comprises the resonances with $\hbar\omega$, is negligible compared to $\text{Im}[A_{ijk}]$, and thus is not included in Fig. 4(b). Also, Eq. (9) presents the phenomenon of *double resonance* [28] in the denominator, whereby there is a region in \mathbf{k} -space where $\epsilon_{nv}(\mathbf{k}) = 2\epsilon_{cv}(\mathbf{k}) = 2\hbar\omega$ (for a given $n \neq c$), which makes the entire perturbation expansion inapplicable. In our calculations this happens for $c = 2$, $v = 1$ and $n = 3$. Figure 4(c)

shows that this double resonance appears around the M point. This troublesome term makes the convergence of $\text{Im}[B_{ijk}]$ unattainable, specially for energies just above the threshold $\min[\epsilon_{cv}(\mathbf{k})]/2$. However, this contribution has been shown to be small and does not affect the nonlinear susceptibility at lower frequencies [4].

VIII. CONCLUSIONS

It has been shown that in a minimal model of a TMDC, where the Bloch eigenstates are expressed as combinations of d orbitals only, the optical response can be obtained with reasonable accuracy, as compared with plane waves *ab initio* models. This is more evident at lower optical frequencies, where most optical experiments are carried out. The key element here is that the tight-binding Hamiltonian written is this approximation matches well *ab initio* results, something that translates into the Bloch wavefunction and the optical response. This calculation takes full advantage of the symmetry of the crystal, in a manner more explicitly displayed as compared to other references.

IX. ACKNOWLEDGMENTS

This project started as a byproduct of another, larger project on nonlinear optics funded by the Department of Energy. I would like to express my gratitude to Luis Enrique Rosas-Hernandez for providing me the SIESTA pseudo orbitals of tungsten.

Appendix A: Liu's three-band model for TMDC monolayer

Liu *et al* [2] have set up a minimal TB model for the whole family of $2H$ TMDCs monolayers including only the transition metal d orbitals that are even under the σ_h mirror operation (d_{z^2} , d_{xy} and d_{x^2}). When including hopping terms up to third nearest neighbors, the resulting TB Hamiltonian reproduces well the uppermost valence and two lowest conduction bands over the entire BZ. In the basis of Bloch sums given by Eq. (10), this Hamiltonian can be written as:

$$H = \begin{pmatrix} h_{11} & h_{12} & h_{13} \\ h_{12}^* & h_{22} & h_{23} \\ h_{13}^* & h_{23}^* & h_{33} \end{pmatrix}. \quad (\text{A1})$$

The D_{3h} point group of the material constrains the number of independent hopping integrals to just nineteen, indicated in Table I. By defining $\alpha = ak_x/2$ and $\beta = a\sqrt{3}k_y/2$ [a is the lattice constant, see Fig. 1(a)], the matrix elements of Eq. (A1) are given by:

$$h_{11} = \varepsilon_1 + 2t_0(2\cos\alpha\cos\beta + \cos 2\beta) + 2r_0(2\cos 3\alpha\cos\beta + \cos 2\beta) + 2u_0(2\cos 2\alpha\cos 2\beta + \cos 4\alpha), \quad (\text{A2})$$

$$\begin{aligned} h_{22} = & \varepsilon_2 + (t_{11} + 3t_{22})\cos\alpha\cos\beta + 2t_{11}\cos 2\alpha + 4r_{11}\cos 3\alpha\cos\beta + 2(r_{11} + \sqrt{3}r_{12})\cos 2\beta \\ & + (u_{11} + 3u_{22})\cos 2\alpha\cos 2\beta + 2u_{11}\cos 4\alpha, \end{aligned} \quad (\text{A3})$$

$$\begin{aligned} h_{33} = & \varepsilon_2 + (3t_{11} + t_{22})\cos\alpha\cos\beta + 2t_{22}\cos 2\alpha + 2r_{11}(2\cos 3\alpha\cos\beta + \cos 2\beta) \\ & + \frac{2}{\sqrt{3}}r_{12}(4\cos 3\alpha\cos\beta - \cos 2\beta) + (3u_{11} + u_{22})\cos 2\alpha\cos 2\beta + 2u_{22}\cos 4\alpha, \end{aligned} \quad (\text{A4})$$

$$\begin{aligned} h_{12} = & -2\sqrt{3}t_2\sin\alpha\sin\beta + 2(r_1 + r_2)\sin 3\alpha\sin\beta - 2\sqrt{3}u_2\sin 2\alpha\sin 2\beta \\ & + 2it_1\sin\alpha(2\cos\alpha + \cos\beta) + 2i(r_1 - r_2)\sin 3\alpha\cos\beta + 2iu_1\sin 2\alpha(2\cos 2\alpha + \cos 2\beta), \end{aligned} \quad (\text{A5})$$

$$\begin{aligned} h_{13} = & 2t_2(\cos 2\alpha - \cos\alpha\cos\beta) - \frac{2}{\sqrt{3}}(r_1 + r_2)(\cos 3\alpha\cos\beta - \cos 2\beta) + 2i\sqrt{3}u_1\cos 2\alpha\sin 2\beta \\ & + 2u_2(\cos 4\alpha - \cos 2\alpha\cos 2\beta) + 2i\sqrt{3}t_1\cos\alpha\sin\beta + \frac{2i}{\sqrt{3}}(r_1 - r_2)\sin\beta(\cos 3\alpha + 2\cos\beta), \end{aligned} \quad (\text{A6})$$

$$\begin{aligned} h_{23} = & \sqrt{3}(t_{22} - t_{11})\sin\alpha\sin\beta + 4r_{12}\sin 3\alpha\sin\beta + \sqrt{3}(u_{22} - u_{11})\sin 2\alpha\sin 2\beta \\ & + 4it_{12}\sin\alpha(\cos\alpha - \cos\beta) + 4iu_{12}\sin 2\alpha(\cos 2\alpha - \cos 2\beta). \end{aligned} \quad (\text{A7})$$

[1] G. G. Macfarlane and V. Roberts, Infrared absorption of germanium near the lattice edge, *Phys. Rev.* **97**, 1714 (1955).

[2] G.-B. Liu, W.-Y. Shan, Y. Yao, W. Yao, and D. Xiao,

TABLE I. Tight-binding parameters from [2] for WS_2 with a generalized gradient approximation (GGA). All values are in eV.

t_0	t_1	t_2	t_{11}	t_{12}	t_{22}
-0.175	-0.090	0.611	0.043	0.181	0.008
r_0	r_1	r_2	r_{11}	r_{12}	u_0
0.075	-0.282	0.356	2.015	2.014	2.056
u_1	u_2	u_{11}	u_{12}	u_{22}	
2.045	0.659	3.014	0.457	0.478	
ε_1	ε_2				
0.717	1.916				

Three-band tight-binding model for monolayers of group-VIB transition metal dichalcogenides, *Phys. Rev. B* **88**, 085433 (2013).

- [3] M. L. Trolle, G. Seifert, and T. G. Pedersen, Theory of excitonic second-harmonic generation in monolayer MoS_2 , *Phys. Rev. B* **89**, 235410 (2014).
- [4] J. L. Cabellos, B. S. Mendoza, M. A. Escobar, F. Nastos, and J. E. Sipe, Effects of nonlocality on second-harmonic generation in bulk semiconductors, *Phys. Rev. B* **80**, 155205 (2009).
- [5] E. Ghahramani, D. J. Moss, and J. E. Sipe, Full-band-structure calculation of second-harmonic generation in odd-period strained $(\text{Si})_n/(\text{Ge})_n$ superlattices, *Phys. Rev. B* **43**, 8990 (1991).
- [6] J. E. Sipe and E. Ghahramani, Nonlinear optical response of semiconductors in the independent-particle approximation, *Phys. Rev. B* **48**, 11705 (1993).
- [7] D. J. Moss, E. Ghahramani, J. E. Sipe, and H. M. van Driel, Empirical tight-binding calculation of dispersion in the linear optical properties of tetrahedral solids, *Phys. Rev. B* **34**, 8758 (1986).
- [8] L. A. Hemstreet and C. Y. Fong, Electronic band structure and optical properties of 3C-SiC, BP, and BN, *Phys. Rev. B* **6**, 1464 (1972).
- [9] J. D. Jackson, *Classical Electrodynamics*, 3rd ed. (Wiley, New York, NY, 1998).
- [10] M. A. Khan and M. N. Leuenberger, First-principles study of the electronic and optical properties of Ho_M impurities in single-layer tungsten disulfide, *Scientific Reports* **12**, 11437 (2022).
- [11] K. F. Riley, M. P. Hobson, and S. J. Bence, *Mathematical Methods for Physics and Engineering*, 3rd ed. (Cambridge University Press, Cambridge, 2006) p. 864.
- [12] G. Y. Guo and J. C. Lin, Systematic ab initio study of the optical properties of BN nanotubes, *Phys. Rev. B* **71**, 165402 (2005).
- [13] G. Lehmann and M. Taut, On the numerical calculation of the density of states and related properties, *Phys. Status Solidi B* **54**, 469 (1972).
- [14] R. W. Boyd, *Nonlinear optics*, 4th ed. (Academic Press, 2020).
- [15] R. Zu, B. Wang, J. He, J.-J. Wang, L. Weber, L.-Q. Chen, and V. Gopalan, Analytical and numerical modeling of optical second harmonic generation in anisotropic crystals using SHAARP package, *npj Comput. Mater.* **8**, 246 (2022).
- [16] L. Liu, Y. P. Feng, and Z. X. Shen, Structural and electronic properties of h-BN, *Phys. Rev. B* **68**, 104102 (2003).
- [17] M. Tinkham, *Group Theory and Quantum Mechanics* (McGraw-Hill, Mineola, New York, 1964).
- [18] L. D. Landau and E. M. Lifshitz, *Quantum Mechanics: non-relativistic theory* (Pergamon Press, Oxford, 1977).
- [19] B. Adolph, J. Furthmüller, and F. Bechstedt, Optical properties of semiconductors using projector-augmented waves, *Phys. Rev. B* **63**, 125108 (2001).
- [20] C. Kittel, *Quantum Theory of Solids* (Wiley, New York, 1963).
- [21] Y. R. Shen, *The Principles of Nonlinear Optics* (Wiley, New York, 1984).
- [22] D. J. Chadi and M. L. Cohen, Special points in the Brillouin zone, *Phys. Rev. B* **8**, 5747 (1973).
- [23] J. C. Slater and G. F. Koster, Simplified LCAO method for the periodic potential problem, *Phys. Rev.* **94**, 1498 (1954).
- [24] J. M. Soler, E. Artacho, J. D. Gale, A. García, J. Junquera, P. Ordejón, and D. Sánchez-Portal, The SIESTA method for ab initio order-N materials simulation, *J. Condens. Matter Phys.* **14**, 2745 (2002).
- [25] M. Methfessel and A. T. Paxton, High-precision sampling for Brillouin-zone integration in metals, *Phys. Rev. B* **40**, 3616 (1989).
- [26] J. Callaway, *Quantum Theory of the Solid State*, 2nd ed. (Academic Press, Inc., San Diego, CA, 1991) p. 557.
- [27] C.-Y. Wang and G.-Y. Guo, Nonlinear optical properties of transition-metal dichalcogenide MX_2 ($\text{M}=\text{Mo, W}$; $\text{X}=\text{S, Se}$) monolayers and trilayers from first-principles calculations, *The Journal of Physical Chemistry C* **119**, 13268 (2015).
- [28] F. Nastos, B. Olejnik, K. Schwarz, and J. E. Sipe, Scissors implementation within length-gauge formulations of the frequency-dependent nonlinear optical response of semiconductors, *Phys. Rev. B* **72**, 045223 (2005).